# An innovative approach towards defect detection and localization in gas pipelines using integrated in-line inspection methods

Santhakumar Sampath [a], Kanhaiya Lal Chaurasiya [a], Pouria Aryan [b], Bishakh Bhattacharya [a,*]

[a] Department of Mechanical Engineering, Indian Institute of Technology Kanpur, Kanpur, 208016, India
[b] School of Electrical & Electronic Engineering, University of Adelaide, Adelaide, SA, 5005, Australia

## ARTICLE INFO

## ABSTRACT

The current study presents a novel and high-sensitivity in-line inspection (ILI) method for gas pipelines. The proposed method is based on integrated ILI methods, optical sensor and bimorph sensor. The uniqueness of the proposed method lies in; (1) combining two advanced methods for more accurate and sensitive outcome, (2) real-time inspection of target pipeline, (3) specifically designed sensor array to estimate and locate defects in three dimensions, and (4) low power consumption and economic viability. The theoretical framework for the relationship between the sensor outputs and the presence of defect as well as the design of the sensor housing module are also developed and presented. Laboratory tests are conducted on various types of defects to illustrate the robustness and sensitivity of the method. Additionally, the conventional magnetic flux leakage (MFL) method is adopted to verify the effectiveness of the proposed method. Furthermore, for the real-world application purposes, a smart pipeline inspection gauge (smart PIG) with integrated different sensor arrays are developed for the field testing of gas pipeline networks. The two-dimensional (2-D) image produced by the sensor array is presented to visualize the inner surface of the pipeline and enable accurate identification of bolted pipe joints. A speed control system is also developed and designed to eliminate errors caused by speed spikes and maintain the speed of the smart PIG within the desired range. An analysis of the chatter vibration signal of the smart PIG running in a gas pipeline network is presented. The current research work provides a solid base towards a step change from a pilot study to a real-time, real-world application of a novel inspection method for pipelines.

## 1. Introduction

Pipelines are the key components to transfer fluids such as oil and gas over long distances. Pipelines serve as assets to the economy of every nation. In India only, at the end of 2018 over 13,000 km of oil and gas pipelines have been installed (Ogai and Bhattacharya, 2018) and this number will be 27,000 km by the end of 2030 (Dhar and Shukla, 2015). Pipeline failure and rupture can be seriously catastrophic and may result in significant economic or human loss. According to statistics published by Pipeline and Hazardous Materials Safety Administration in the USA, a total of 1969 accidents of oil and gas pipelines are reported worldwide from 2010 to 2018 (Eybpoosh et al., 2017; Amaya-Gómez et al., 2019). These accidents caused 357 injuries, 59 fatalities and incurred a cost of almost $518 million. The most common causes of the failures are reported to be corrosion, crack, dent, deposit and metal loss (Iqbal et al., 2017; Askari et al., 2019). The causes can happen due to construction defects, third-party damage or environmental factors (severe temperature conditions, earthquakes, and rough seas) (Xie and Tian, 2018; Ho et al., 2020). Rapid development of oil and gas industry in recent years and future requires more reliable inspection methods to maintain the integrity and operability of the pipeline.

Amongst the all non-destructive developed tools, In-line inspection (ILI) methods are one of the most commonly used tools for safe maintenance of pipelines (Bickerstaff et al., 2002). The ILI tools facilitate the inspection and defect detection since they are mounted on the pipeline inspection gauges (PIGs), which are autonomous inspection robots (Okamoto et al., 1999; Dong et al., 2019). The PIGs are normally propelled inside the pipeline using the kinetic energy of oil and gas transmission medium and perform the inspection without service disruption or damaging the pipeline. The most common methods for ILI purposes are magnetic flux leakage (MFL) (Wu et al., 2020; Peng et al., 2020), ultrasonic testing (UT) (Nakhli Mahal, 2020; Salama et al., 2013), eddy current (EC) (Xie et al., 2020), electromagnetic acoustic transducers (EMAT) (Mikhaylov et al., 2020; Wang et al., 2020) and pulsed eddy

---

\* Corresponding author.
*E-mail address:* bishakh@iitk.ac.in (B. Bhattacharya).

current (PEC) (Zhao et al., 2020; Xue et al., 2020). In MFL, the disturbance in magnetic flux is the sign of defect presence. MFL is the most common method however it is limited to ferromagnetic material-based and certain wall thicknesses and diameters of pipes (Gloria et al., 2009). As one of the most accurate methods, UT, utilizes ultrasonic wave reflection to assess the integrity of the pipeline. Two major constraints of UT are the use only in oil pipelines due to the good acoustic properties and the inspection speed which cannot be more than 2.5 m/s (Reber et al., Barbian; Caleyo et al., 2007; Sampath et al., 1051). The EC method uses deep magnetic penetration in ferromagnetic material-based pipelines and is sensitive to internal defects. However, EC can produce inaccurate results due to spacing problem in mounting the sensor array on the circumference of the PIG (Varela et al., 2015; Ulapane et al., 2017). Another major challenge in EC method is to maintain the sensor lift-off (i.e., distance between the location of sensor and the inner surface of the pipeline). EMAT is relatively a new method and same as UT, is working based on generation of ultrasonic waves through the Lorentz forces. The main limitations of EMAT are; very small lift-off distance (less than 1 mm) which can seriously affect the fluid flow and the method cannot be utilized for gas pipelines due to poor acoustic properties (Xie and Tian, 2018; Li et al., 2018). PEC method consists of excitation coil and magnetic sensor. The output response contains a broad frequency spectrum. The defect information such as depth, length and thickness can be extracted from the spectrum. However, significantly higher operation cost compared to other methods such as MFL is a serious drawback (Sophian et al., 2002; Xie et al., 2019). In addition, PEC is also limited to 2.5 m/s scanning speed for inspection purposes.

More advanced ILI methods such as closed-circuit television (CCTV) (Duran et al., 2002) and mechanical contact probe (MCP) (Li et al., 2015a; Saeidbakhsh et al., 2009) have been recently developed to address the requirements of the industry. CCTV method captures high-quality images and videos from the surface of the pipeline and through image processing can assess the recorded data. Consequently, it requires a high-power supply and may show resolution ambiguity (Duran et al., Seneviratne). Additionally, complex image-processing tool and significant on-board programming to analyze output data and distinguish the details of the defects are the necessities (Hawari et al., 2018). MCP is a contact method, which works based on the angular variation of inspected arm, so that any angular variation generated by an internal defect is recorded and used to detect dent or deposit (Li et al., 2015b; Zhu et al., 2018). Compared to other ILI methods, the MCP has advantages such as direct contact with the surface of pipe and much lower operation costs also the inspection ability for complex geometry pipes (e.g., curved pipeline). However, the method is not quite robust for metal loss detection, and the friction involved in the inspection process is a risk factor (Yu et al., 2005).

To detect more defect types, have high sensitivity and accurate detection and localization of the defects, the current paper proposes a novel ILI method, which can be installed on smart PIG. The primary concept of the proposed method is to integrate two inspection methods (a non-contact and a contact) together and benefit from the advantages and improve the current limitations of inspection methods. The proposed method consists of an optical sensor array and a bimorph sensor array. The inspection principle of the proposed method and their basic theoretical formulation is presented. The design and hardware components of each method have been developed. Initially, different types of defects, viz., convex defects and metal loss, have been considered to validate the robustness of the proposed method. The experimental variables and uncertainties which influence the accuracy of the measurements have been studied. To provide a solid baseline for the outcomes of the proposed method, the results are compared with the outcomes from the conventional MFL method for the same experimental conditions. For the next step, the smart PIG carrying integrated ILI modules is tested in a networked gas pipeline for simulation of the real field application. A speed control module is designed to maintain and control the speed of the smart PIG so that different ILI modules can inspect the pipeline at a

optimum constant speed to avoid false identification errors. Finally, an analysis of the chatter vibration signal of the smart PIG running in a gas pipeline network is presented. The smart PIG is installed odometer self-location unit to measure or tag the position of the detected defects. The uniqueness of the current study are described in the following:

(1) The advancement of the integrated ILI methods (optical sensor and bimorph sensor) which are capable of detecting all types of common defects to the best of authors' knowledge as there is no single ILI method currently available to detect all types of defects in pipelines. Both the proposed methods have no practical limits of wall thickness and capable of damage detection in both oil and gas pipelines. The methods are equally applicable for ferrous as well as non-ferrous pipe-lines. In contrast to conventional ILI methods, the bimorph sensor provides the direct dimensions of pipeline defects by contact.

(2) The proposed smart PIG inspection module has low power consumption. It is cost-effective, easy to fabricate and operate as a reliable and robust system for real-world application purposes.

(3) A speed control system is attached to the PIG and moved in the pipeline to control the travel speed of the whole system. The novel feature of the speed controller is that it is a passive, robust and light-weight hydro-mechanical system which can be customized in-line with the desired magnitude of travel velocity. The development of a speed control system for smart PIG helps to accurately identify and classify defects and leakage and metal loss/corrosion detection thereby enhancing the effectiveness of the inspection tool. The entire system does not require any electrically powered motors and hence it is safe and robust for driving pipe inspection robots at a uniform slow speed in an inflammable environment.

(4) Array detection method for real-world application. Most of the published research in the literature have discussed the basic evaluations of one-dimensional (1D) information regarding the defect, such as length, width, or height (Li et al., 2015a; Bubenik et al., Saffell; Ege and Coramik, 2018; Canavese et al., 2015). An array of sensors which is installed around the circumference of the PIG can be elucidated as a "sensor image" of the pipeline surface. The current study presents a sensor array which can be interpreted as a "2D or 3D image" of the pipeline surface which provides more information and results in more accurate detection and localization of the defects.

(5) Real-time inspection of PIG is an important aspect of ensuring the safety of the gas pipeline. The current study proposed smart PIG with the capability of performing real-time inspection of pipelines. The smart PIG is capable of being equipped with a wireless robot tracking system such as X-bee (pro-S1 PCB antenna model), by which the position of the robot and locations of the probable defects could be obtained in real-time. In such a case, two X-bee modules could be used to communicate with each other, where one can be used for the transmission and the other as a receiver. The transmitter X-bee must be mounted on the microcontroller board, while the receiver X-bee via RF (radio frequency) waves receives data using the ZigBee protocol.

The paper is organized as follows: Section 2 discusses the development of the proposed method and conventional MFL method. The housing module of integrated ILI methods and the hardware components and configuration are presented in Section 3. Section 4 provides the laboratory studies, including specimen details, design of the testbed and test results. Section 5 elaborates on the performance of the integrated ILI method in the real test field and describes the speed control system. The conclusions and summary of outcomes of the current research, along with the future directions, are presented in Section 6.

## 2. Development of integrated ILI methods

### 2.1. Optical sensor method

The proposed optical sensor method is based on the absorption of emitted (reflected) optical or visible light and utilization of the optical sensor. This method essentially contains a transmitter and receiver, as shown in Fig. 1. The transmitter is a light-emitting diode (LED) that constantly emits light. The receiver is a light-dependent resistor (LDR) that receives the reflected light back from the inner surface of pipelines. The LED converts electrical energy to optical or light energy, whereas the LDR works on photoconductivity. The emitted light from the LED travels through the medium (e.g., gas) and provides the optical data as reflected from the pipeline wall. The reflected light on LDR often changes the output signal. This signal can be further analyzed by signal processing techniques to extract the information related to defects or surface irregularities.

The intensity of reflected light ($I_r$) is related to the irregularities (i.e., defects) of the pipeline surface ($\sigma$) as described in the following Eq. (1) (Beckmann and Spizzichino, 1987);

$$\frac{I_r}{I_o} = kexp\left[-\left(\frac{4\pi\sigma cos\theta}{\lambda}\right)^2\right] \tag{1}$$

where $k$ is the material constant, $\theta$ is the incident angle of light (which is normal to the surface), $\lambda$ is the wavelength of the transmitter (e.g., green light 510 nm) and $I_o$ is the intensity of the reflected light coming from a defect-free or smooth surface. Eq. (1) shows the correlation between the intensity of the reflected light and the defect. The relationship between the intensity and resistance of reflected light is given by

$$R_r = R_o - k_1 ln\left(\frac{I_r}{I_o}\right) \tag{2}$$

where $R_r$ is the resistance of reflected light, $R_o$ is the incident light and $k_1$ is the proportionality's constant. The circuit diagram shown in Fig. 1(c) is used to connect the receiver. The resistance of the receiver changes in proportion with the variation of the light intensity and is connected to the input voltage $V_{in}$ followed by a fixed resistor in series. The output voltage $V_{Optical}$ across the sensor is measured using the voltage divider circuit governed by Eq. (3),

$$V_{Optical} = V_{in}\left(\frac{R_{LDR}}{R_{LDR} + R}\right) \tag{3}$$

where R is the resistance of the fixed resistor and $R_{LDR}$ is the resistance of the sensor. A detailed description of the developed theoretical work has been provided in the previous publication (Sampath et al., 2019) and only basic principle and mathematical relation are presented here.

### 2.2. Bimorph sensor method

The bimorph sensor method is developed and designed based cantilever smart probe method for detection, localization, and sizing of surface defects. This method is based on the principle of piezoelectricity and comprises three elements, including the bimorph sensor, probe tip, and cantilever beam made of glass fiber, as shown in Fig. 2. The bimorph sensor is patched to the cantilever beam to measure the dynamic strain of the cantilever as it encounters defects while passing through the pipeline (Sampath et al., 2020). The defects or irregularities that intervene are sensed as the soft probe touches the defects and is deformed (shown in Fig. 2(b)). The bending strain produces the mechanical energy in the bimorph sensor. The sensor converts the mechanical energy (dynamic strain) to electrical energy (voltage). Conversely, when there is no defect in the pipelines, the sensor moves along without any deformation. The electric circuit diagram of the sensor is illustrated in Fig. 2(c).

The bimorph is piezoelectric material and follows a linear piezoelectric theory, which couples electrical charges in response to mechanical stress. The bimorph consists of two layers of piezoelectric material connected over their length surfaces. The bimorphs are usually supplied in a thin film, typically ranging from 9 to 110 μm thickness. A minute bending (mechanical stress) in the cantilever results in a high
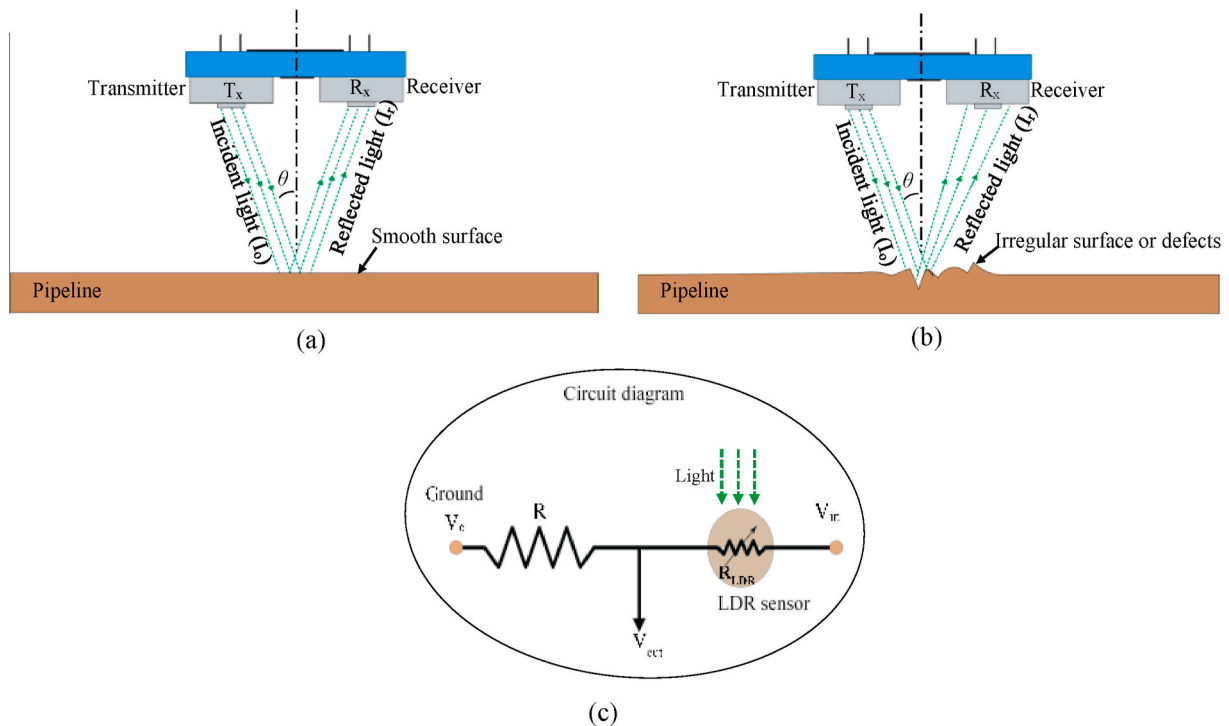


**Fig. 1.** The complete procedure of the optical sensor method: (a) schematic of the optical sensor without defects, (b) optical sensor with defects and (c) the electric circuit diagram.
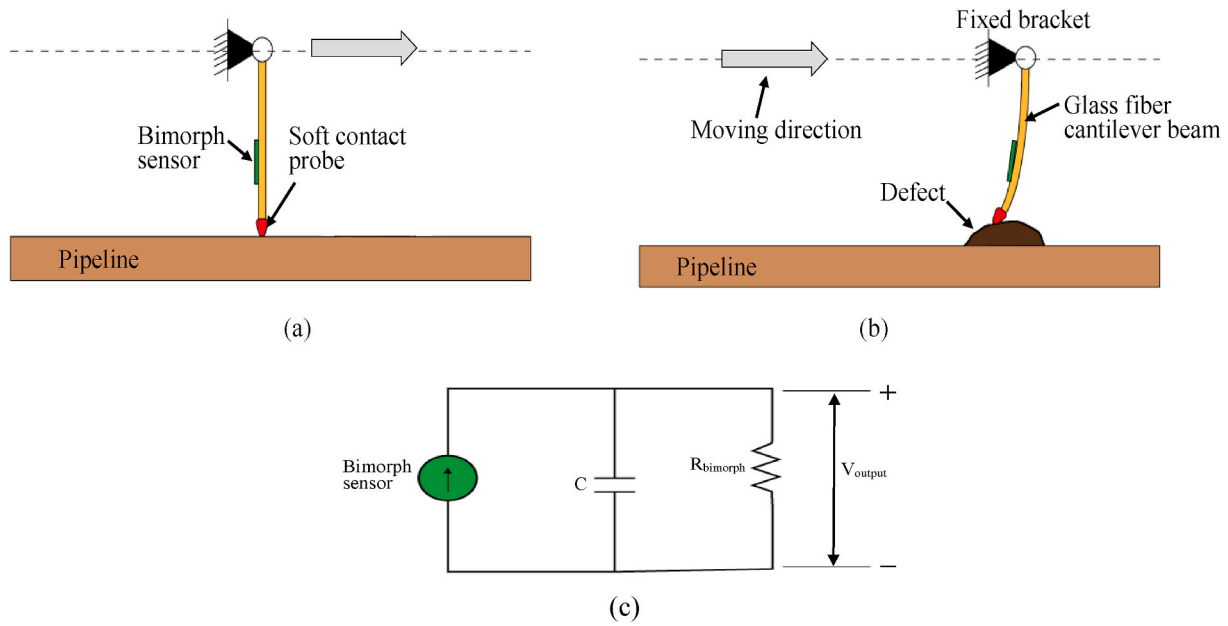
**Fig. 2.** Inspection principle of the proposed bimorph sensor method: (a) pipeline without defect (b) pipeline with the defect and (c) circuit diagram of the bimorph sensor.

voltage output due to the small cross-section area. The bimorph is a low-cost micromechanical sensor for measuring strain on the cantilever beam (Lim et al., 2005). The sensor senses dynamic strain produced due to defects and gives the voltage value corresponding to the rate of strain change. The cut-off frequency of the bimorph is calculated based on Eq. (4).

$$f_c = \frac{1}{2\pi\Omega C} \tag{4}$$

where $\Omega$ is the load resistance, and $C$ is the sensor's capacitance. The output response of the sensor is proportional to the dynamic change of strain (in this case, produced by a defect in the pipeline). The output voltage of the sensor is expressed as in equation (Agarwal et al., 2011),

$$V_{bimorph} = G\frac{dQ(t)}{dt} = G\{K_s\}^T\{\dot{\varepsilon}\} \tag{5}$$

where $G$ is the constant gain of the charge amplifier, $Q(t)$ is the bimorph charge, $\{K_s\}^T$ is a global coordinate system corresponding to the spatial integration of a complex function over the surface of the bimorph sensor, and $\{\dot{\varepsilon}\}$ is the strain rate due to the presence of a defect in the pipeline. The electrical equivalent of the sensor in the charge mode is equal to a charge source in parallel with a capacitance represented by a charge amplifier (Kursu et al., 2009). Now, from the theory of a cantilever beam, for external load ($P$) at the end tip of a beam or soft contact probe and fixed at the one end, deflection at distance ($x$) is given by Eq. (6).

$$\delta = \frac{PLx^2}{2EI} - \frac{Px^3}{6EI} \tag{6}$$

where $L$ is the length of the cantilever beam, $\delta$ is the deflection due to defects, $E$ is the modulus of the elasticity and $I$ is the area moment. Consider a bimorph attached at a distance $l$ from the tip of the cantilever beam. Due to defects, there is a certain strain produced at this position; then dynamic strain ($\varepsilon$) developed due to defects can be expressed as Eq. (7).

$$\varepsilon = \frac{3\delta lt}{2L^3} \tag{7}$$

where $t$ is the thickness of the cantilever beam and $\delta$ is the deflection due to defects. This relation is obtained from the moment curvature rela-

tionship for deflection. By substituting Eq. (7) into Eq. (5), the output response of the bimorph sensor can be obtained. Eq. (5) shows that the output voltage of the bimorph sensor is always proportional to the strain produced in the cantilever beam due to the defects.

### 2.3. MFL sensor method

The basic working principle of the MFL method is that the entire circumference of the pipeline-wall made of ferromagnetic material is magnetized close to saturation by the induced magnetic field (Smith and Hay, 2000). The presence of defects such as metal loss distorts the magnetic flux lines which will be sensed by the Hall sensor (Fig. 3).

The magnetic field generated by the magnetizer is governed by (Li et al., 2006)

$$\nabla \times \frac{1}{\mu}(\nabla \times A) = J - \sigma\frac{\partial A}{\partial t} + \sigma v \times (\nabla \times A) \tag{8}$$

where $A$ is the magnetic vector potential ($B = \nabla \times A$), $\mu$ is the permeability, $\sigma$ is the conductivity, $J$ is the source current density and $v$ denotes velocity. The output Hall voltage $V_{Hout}$ is expressed by Eq. (9).

$$V_{Hall\ sensor} = R_H\left[\frac{I}{t}B\right] \tag{9}$$

where $R_H$ is the Hall effect co-efficient, $I$ is the current flow through the sensor in amps, $t$ is the thickness of the sensor in mm and $B$ is the Magnetic flux density in Teslas. The charge carriers experience Lorenz force since the magnetic field with magnetic flux density (B) is present and the field direction is perpendicular to the motion of the charge carriers. The response of the Lorenz force creates output Hall voltage, recorded using a data acquisition system. The output data from the DAQ can be analyzed to examine the condition of the pipeline.

## 3. Housing module designs and hardware configurations

### 3.1. Optical sensor module

The designed housing module of the optical sensor consists of 32 transmitters and 32 receivers that are mounted over the circumference of the head of the housing module as shown in Fig. 4. The outer diameter
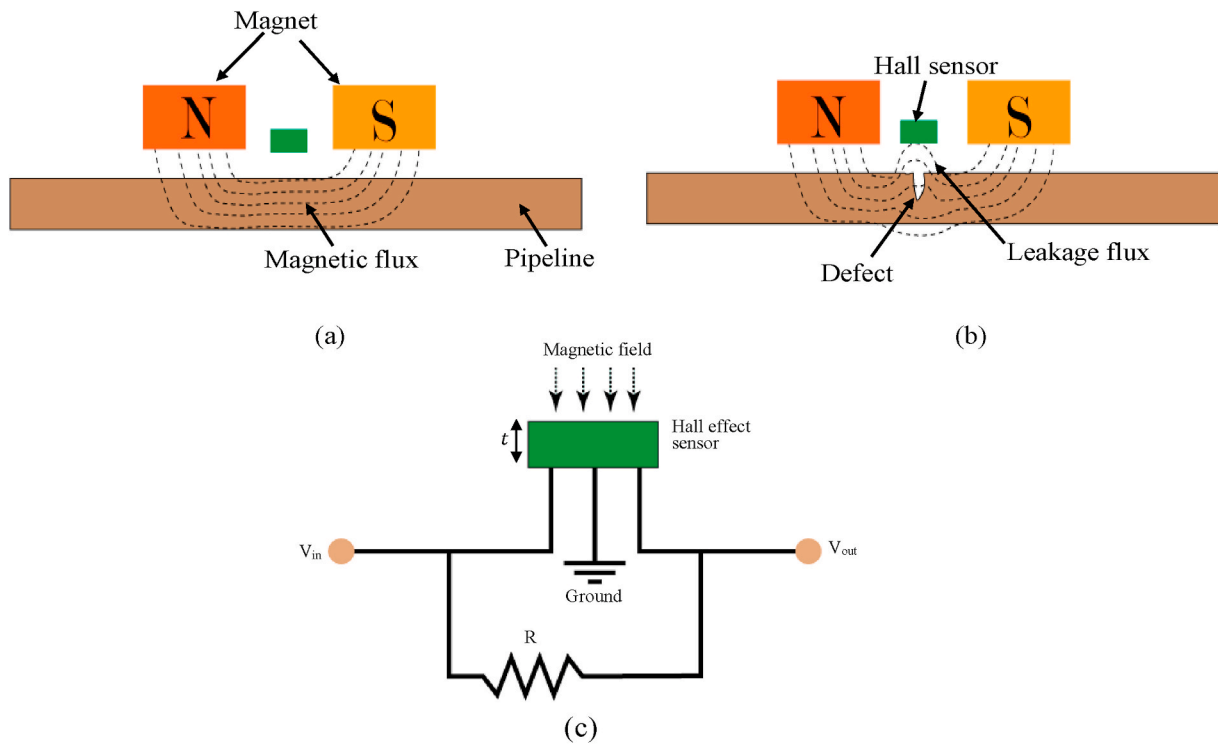
**Fig. 3.** Working principle of MFL sensor method (a) pipeline without defect, (b) pipeline with a defect and (c) electric circuit diagram of the MFL sensor.
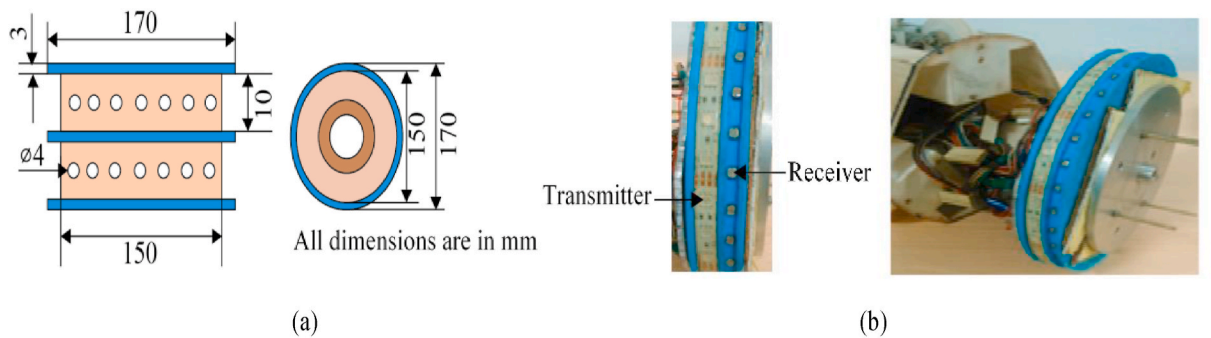


**Fig. 4.** The sensor module dimensions and components (a) different views with sizes and (b) the photo of the housing module with the locations of the transmitter and receiver.

of the housing module is 170 mm, while the inner diameter of the gas pipe is 200 mm. In case of the 32 transmitters and 32 receivers, since the current pipeline under inspection inner has diameter of 200 mm and considering the dimensions of the transmitters and receivers and the associated distances between them, 32 is the optimum number of the transmitters and receivers to perfectly cover the whole surface of the pipeline. In case of pipelines with different diameter, the system is quite flexible and can be customized and adjusted for the required diameter. A gap of 15 mm is sufficient for the gas to flow through the pipe. The transmitters used a green light LED model from the series with 170 mm length, EST-312-G20 made by Elstar Electronic Co., Ltd. China. The receivers are cadmium sulfide (CdS) LDR (model GL55, Nanyang Senba Optical and Electronic Co., Ltd, China). The electrical properties of the transmitter and receiver are listed in Table 1. The price for an optical sensor is approximately $ 3 for each pair of transmitter and receiver and the required power is 2.5 mW for each sensor. The sensors are optimally positioned to measure the intensity of the reflected light. The sensors and emitters are 5.3 mm apart. To increase the reflected intensity of light, the angle of the incident transmitter is set at zero, normal to the surface of the pipeline. Both transmitters and receivers operate

**Table 1**
Electrical properties for the optical sensor.

| Parameters | LED transmitter | LDR receiver |
|---|---|---|
| Dimension | $4 \times 8 \times 2.4$ mm | $6.5 \times 5.5 \times 4$ mm |
| Voltage | 12 V | 5 V |
| Power Consumption | 24 mW | – |
| Dark Resistance | – | 1 M$\Omega$ |
| Power Dissipation | – | 100 mW |
| Operating Temperature | $-30\,°C \sim 85\,°C$ | $-30\,°C \sim 70\,°C$ |
| Response time | – | Rise time 20 ms Decay time 30 ms |
| Relative sensitivity of CdS for the green LED | – | 100% |

simultaneously (or "Switched ON" at the same time).

### 3.2. Bimorph sensor module

The bimorph is made of the piezoelectric ceramic element (EB-T-320 model, Low Power Radio Solutions Co., Ltd., United Kingdom). The bimorph cost 4 \$/each and is well suited for defects inspection in long-distance pipelines. The four bimorph sensors are circumferentially enclosed by the four arms of the housing module and the distance between the sensors is set to 50 mm (see Fig. 5). The dimension of the bimorph sensors is $15 \times 1.5 \times 0.6$ mm in length, width, and thickness. The size of the glass fiber cantilever beam is $39 \times 31$ mm. For the better stiffness, the design of the cantilever beam is set to be of rectangular shape (cross-section) with a V-shaped tip edge (Biswal et al., 2017). To avoid friction between the cantilever beam and pipeline surface, the probe tip is made of Nylon having relatively lower coefficient of friction. The dimension of the probe tip is $10 \times 10$ mm$^2$. The technical specifications of the bimorph sensor are listed in Table 2.

### 3.3. MFL sensor module

The housing module of the MFL unit consists of two parts – the magnets (two poles) and the Hall sensor (Fig. 6). The MFL housing module maintains a gap of 5 mm from the inner surface of the pipeline wall for easy bypass flow of the fluid and ensures an optimum flux leakage as well. The Hall sensor is the SS49E model supplied by Honeywell International Electronic with a sampling rate of 1 kHz. The MFL housing module with four arms circumferentially spaced at 90° to have an end-to-end diameter of 160 mm. The magnet had a permeability of 300 H/m and relative permeability of 1.05. The experimental parameters of the MFL sensor are listed in Table 3. To minimize the flux leakage between the two magnetic poles, the 40 mm distance is chosen between the magnets and the Hall sensor.

## 4. Laboratory studies

In the laboratory studies, the two main goals are: 1) identification of as many defects as possible within a short length of the pipe specimen, and 2) determination of the ability of the proposed method in identifying different types of defects.

### 4.1. Test specimen

The steel (X80 grade) pipeline with an inner diameter of 200 mm and a wall thickness of 7 mm is selected as the test specimen. Two types of defects such as convexities (e.g., dents) and metal loss are introduced with different sizes as shown in Fig. 7(a). Defects are carefully selected based on the specifications of the common types reported in the literature (Vanaei et al., 2017; Ginzel and Kanters, 2002). Metal loss is an aging defect that is simulated by the electro-erosion process. However, the convexities produced are ideal convex defects of different depths and lengths. The test specimen includes thirteen defects with the geometrical

**Table 2**
Technical specifications of the bimorph sensor.

| Parameters | Bimorph sensor |
|---|---|
| Dimension | $15 \times 1.5 \times 0.6$ mm |
| Voltage | 5 V |
| Capacitance | 750 pF $\pm$ 170 |
| Max stress | 50–100 μm |
| Impedance | 1 M Ω |
| Operational temperature range | - 20–60 °C |

parameters listed in Table 4. Preliminary, convex defects are utilized as the reference to calibrate the proposed ILI method; subsequently, metal loss defects are also introduced to confirm the accuracy of the proposed ILI method.

### 4.2. Test set up

A laboratory testbed is designed to move the housing modules of ILI method along the pipeline (Fig. 7). The optical sensor and MFL sensor modules can move in linear motion using a rack and pinion mechanism. A table-rotation mechanism is also designed to rotate the bimorph sensor modules. The rotary motion for the bimorph sensor method is to produce electrical output during the movement of smart PIG inside the pipeline. The bimorph sensor module remained stationary when the rotary table rotated at constant angular speed. The fluid flow direction exerted the optimal thrust required for the rotation and linear movement of the bimorph sensor module.

The experimental setup consists of three units, viz., the inspection unit, the data acquisition (DAQ) unit, and the data processing unit. The DAQ unit comprised of a DC regulator power supply (12V PSD), microcontroller (Arduino Mega 2560) and motion controller (PCI 7352). A microcontroller controls the movements of the setup. The lift-off distances are approximately 15 mm and 5 mm, for the optical and MFL housing modules, respectively, during the inspection. The inspection speed of the integrating sensor is set to 2.9 mm/s. The radial and tangential components of the MFL signal are measured using a Hall sensor with a resolution of 100 nT. Data on thirteen defects of the specimen are collected and processed where responses 1–6 are convexities and corresponding to 7–13 are metal losses. During the experiments, optical sensor inspection is performed in the dark-room laboratory; to simulate the real pipeline condition and minimize unnecessary errors from ambient lights.

### 4.3. Experimental results

The recorded signals from the optical sensor method for convex defects had depths of 1 mm, 2 mm, and 4 mm with lengths of 31.9 mm, 41 mm, and 50 mm are presented in Fig. 8 (a & b). The output results are plotted in the time domain as well as axial distance. The results suggest that there is a considerable increase in the voltage in case of a convex defect. The experimental results are shown in Fig. 8(a); the minimum
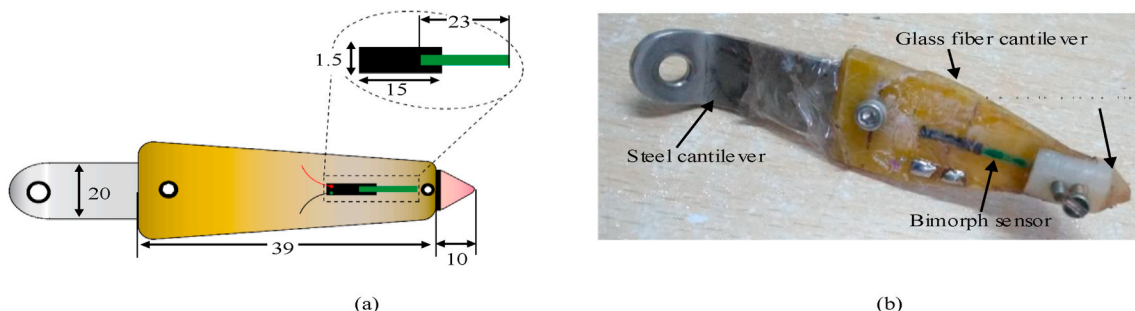


(a)                                        (b)

**Fig. 5.** Schematic diagram of the bimorph sensor housing module (a) 2D view of the bimorph sensor and (b) picture of the bimorph sensor.
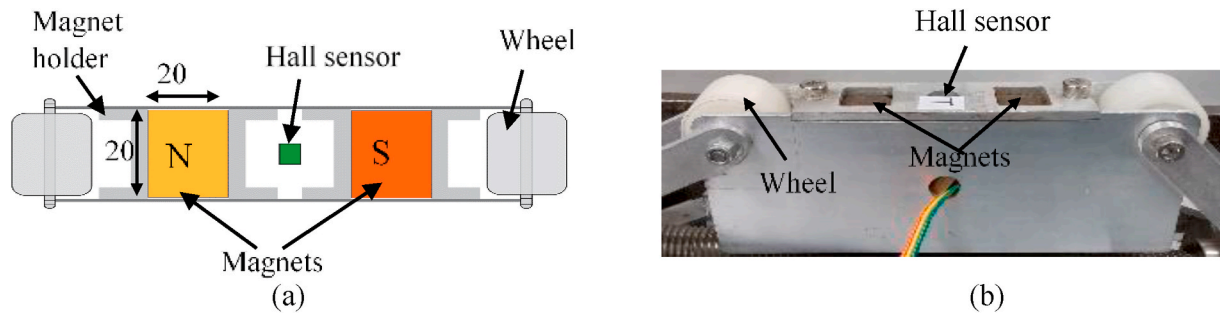
**Fig. 6.** The design of the MFL method (a) schematic diagram of the 2D MFL model and (b) picture of the MFL housing module.

**Table 3**
Characteristics of the MFL method.

| Parameters | Magnet | Hall sensor |
|---|---|---|
| Dimensions | 20 × 20 × 50 mm | 4 × 3 × 1.52 mm |
| Residual flux density | 1170 mT | – |
| Coercive force | 568 kA/m | – |
| Lift-off | 5 mm | 5 mm |
| Voltage | – | 5 V |
| Response time | – | 3 μs |
| Operational temperature range | – | −40–150 °C |

defect detected by the optical sensor had a depth of 1 mm. The convex defect increased the scattering of the incident light, which substantially reduced the intensity of the reflected light. Similar results for metal loss defects of the same length (40 mm) but of different depths (1.5, 1.25 and 1 mm) are presented in Fig. 8(c). The results suggest that the reduction in pipeline thickness by the metal loss defect is closely related to the voltage change of the detected signal. Similarly, Fig. 8(d) shows the optical output signal for three metal loss defects with different defect lengths, i.e., 20 mm, 20 mm, 25 mm, and 15 mm with defect depth kept

constant at 2 mm. The clear peaks are observed at the locations of the metal loss, which are consistent with the lengths of the defects. It is apparent that both the length size and depth of the defects are directly proportional to the voltage obtained from the detected output signals.

To evaluate the performance of bimorph sensor method, the similar convex defects (a1, a2, a3 and b1, b2, b3) are used. The inspection speed is set to 2.9 mm/s and the results are presented in Fig. 9. The distinct output voltage peaks are observed at the locations of the defects. It is observed that the voltage recorded at the instant when the cantilever probe first touches the defect is the highest at 1.5 mm height. This is due to the reason that higher depth of defect causes larger bending of the probe and thus a higher strain is developed hence, a high voltage is recorded in the output. The bimorph sensor method shows sensitivity to the variations of the length and depth so the severity and dimensions of the defect can be measured and evaluate through analyzing the amplitudes of the output voltage.

Since the MFL is one of the most common ILI methods, experiments are performed under the same environmental conditions to validate and verify the proposed method with MFL. The Hall sensor output of the magnetic flux profile for metal loss with different depth is shown in Fig. 10. Distinct changes in the amplitudes of the output voltage show
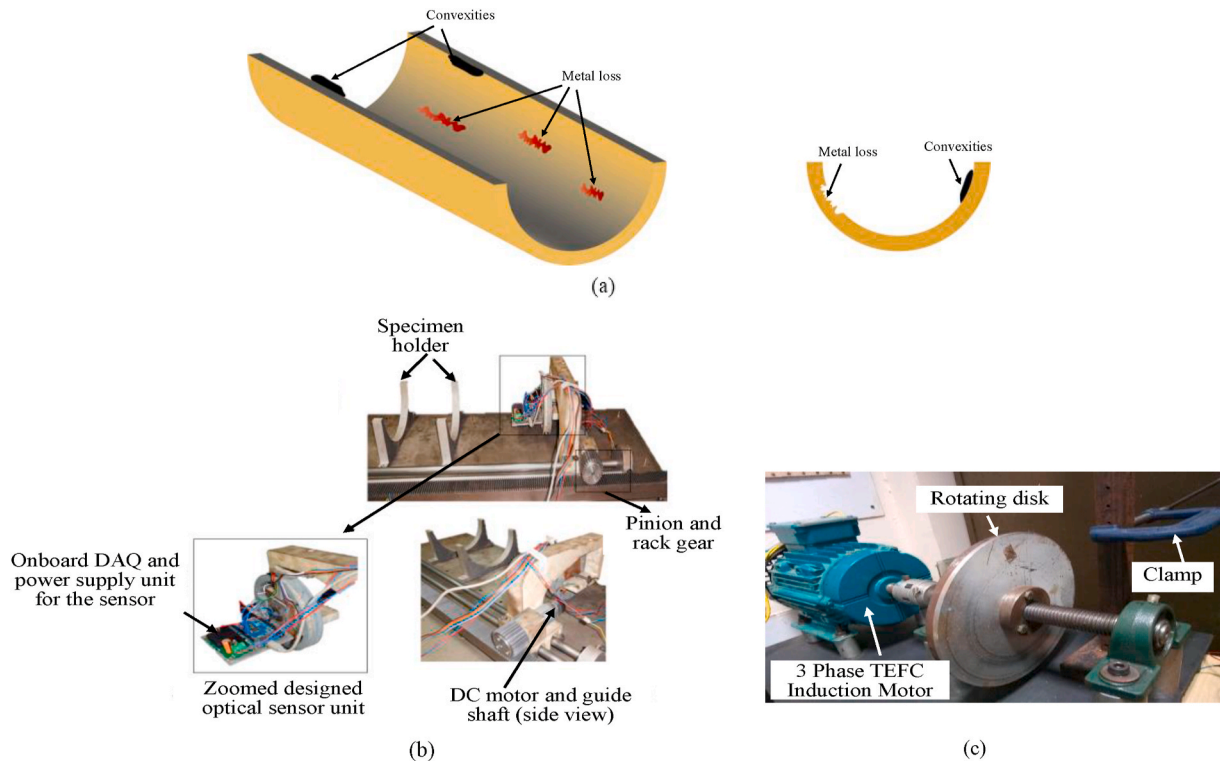


**Fig. 7.** The designed laboratory testbed and the specimen for integrating sensors, (a) different views of the pipe segment with the defects, (b) parts of the rack and pinion mechanism design and (c) rotating mechanism design.

**Table 4**
Geometrical parameters for the defects.

| Category of defects | Convex defects | | Metal loss | |
|---|---|---|---|---|
| No of defects | 3 | 3 | 3 | 4 |
| Size of defects (length, depth) | • a1: 31.9 mm × 1 mm | • b1: 40 mm × 1.5 mm | • c1: 40 mm × 1.5 mm | • d1: 20 mm × 2 mm |
| | • a2: 41 mm × 2 mm | • b2: 40 mm × 1 mm | • c2: 40 mm × 1.25 mm | • d2: 20 mm × 2 mm |
| | • a3: 50 mm × 4 mm | • b3: 40 mm × 1.5 mm | • c3: 40 mm × 1 mm | • d3: 25 mm × 2 mm |
| | | | | • d4: 15 mm × 2 mm |

the locations of the metal loss defects. Both the radial and axial components of the MFL signal illustrate the depth, length, and location of the defect.

### 4.4. Estimation of defect depth and length

The section focuses on estimating the defect size from the output sensor signal. The amplitude of the recorded voltage coincided with the defect sizes (length and depth). For instance, the maximum voltage measured from the optical sensor is 2.345 V, while for the bimorph sensor is 3.145 V. Both sensors measured maximum voltage for a defect

depth of 4 mm. Similarly, the minimum voltage is recorded for 1 mm of defect depth. Fig. 11 shows a linear relationship between the peak voltage of the sensor signal and the defect depth. There is an increase in the response of all the output signal patterns with an increase in the depth of defects. Hence, output signal amplitude is an effective criterion to evaluate defect sizes.

The relationship between the output response and the defect size can be established based on two parameters: the voltage difference between peaks ($\Delta h$) and the difference in position ($\Delta l$). As shown in Fig. 12, $\Delta h$ is calculated for different defect depths (1–4 mm) and similarly, the $\Delta l$ is presented for different lengths of defects (15–50 mm). $\Delta h$ and $\Delta l$ values showed linear proportional to the variation in actual defect size.

The estimated depths and relative errors (RE) are presented in Fig. 13 and Table 5. The relative error (RE) is used to estimate the precision of measurement. The average RE of 13.15% and 11.7% are calculated for the optical sensor and bimorph sensor, respectively. It is evident the lowest RE occurs when the defect depth is maximum. The output response and the expression for estimating the defect depths for the case of conventional MFL are already well established (Kim et al., 2018). The RE for the conventional MFL method is approximately 10.8%. From the results, it is possible to assume that the sensitivity of the proposed bimorph sensor method is slightly lower than the MFL method, however, the proposed bimorph method can give more accurate results in depth defects, which is approximately equal to MFL method. To improve the sensitivity of the optical sensor method further, it is required to maintain the minimum lift-off distance, (i.e., less than 15 mm).

The estimated defect length results and their associated relative errors are shown in Fig. 14 and listed in Table 6. The output results show
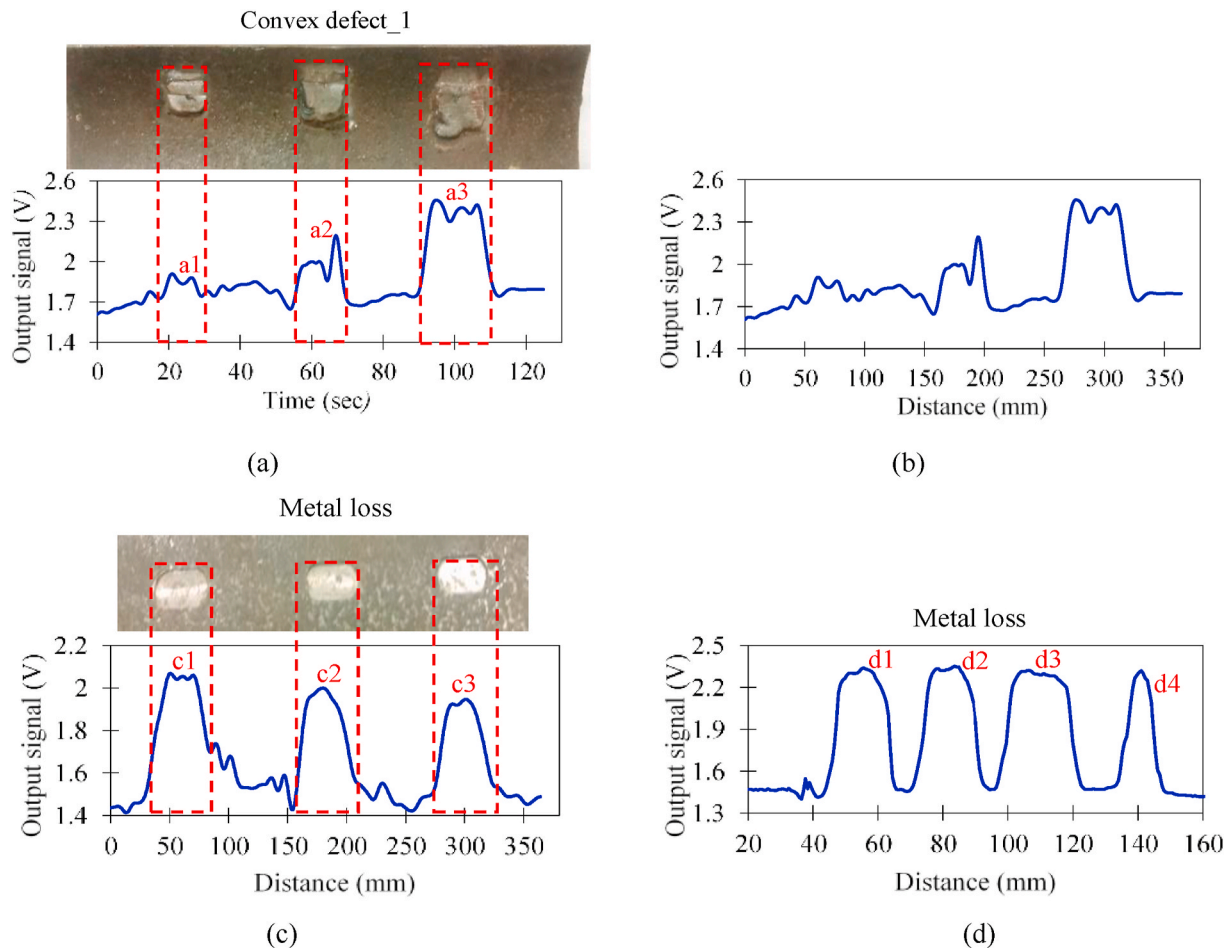


**Fig. 8.** The output response recorded at 2.9 mm/s and 15 mm lift-off (a) time-domain signal for deposited defects and (b) corresponding distance signal (c) metal loss with various depth and (d) metal loss with various width.
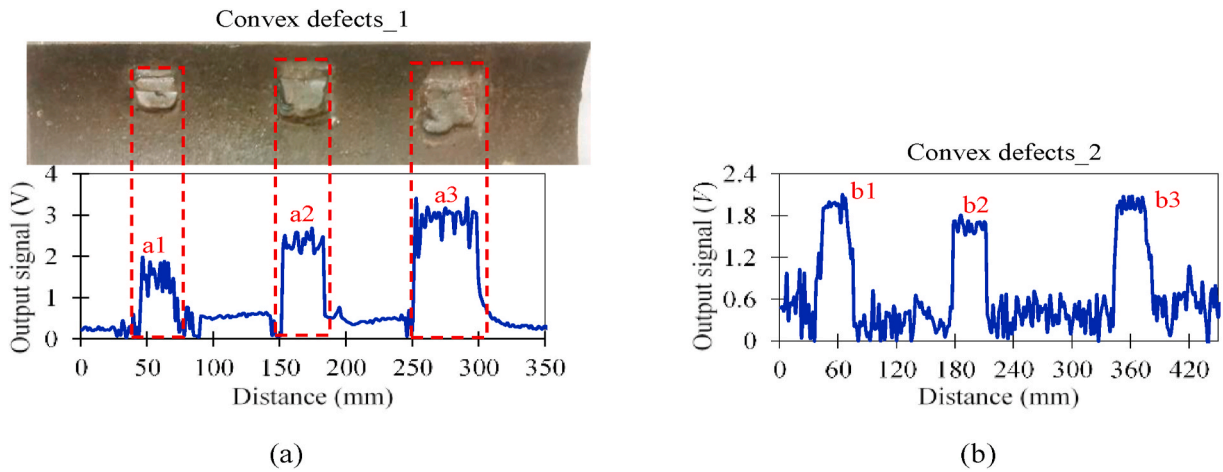
Fig. 9. Experimental results of the bimorph sensor method across convex defects at 2.9 mm/s scanning speed (a) at different lengths of the defects and (b) at different depths of the defects.
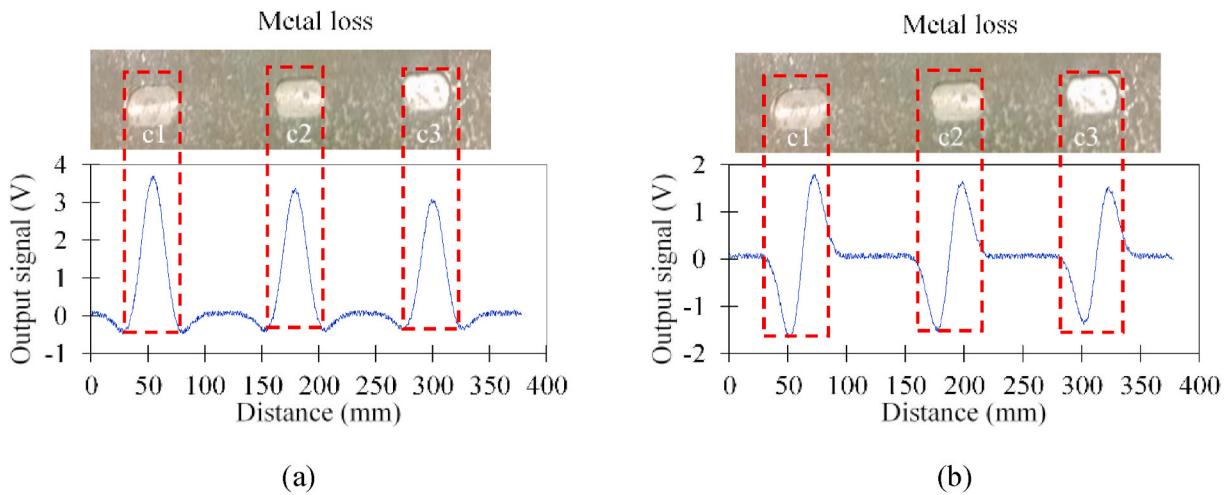


Fig. 10. The magnetic field of metal loss defects with different depths. (a) Axial MFL signals and (b) radial MFL signals.
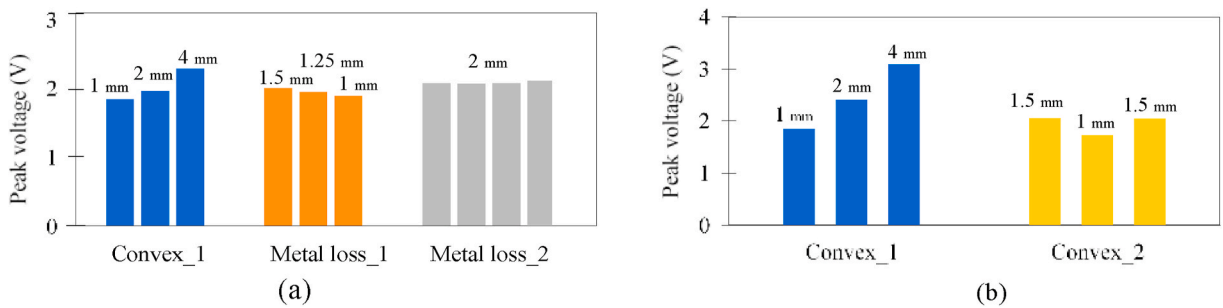


Fig. 11. Peak output voltage for all damaged segmented pipeline at each arrangement, (a) optical sensor method and (b) bimorph sensor method.

that the optical sensor method results are in good agreement with the actual lengths measured. The average RE is less than 7%. However, in the case of the bimorph sensor method, RE is increased to 12.42%. Furthermore, the length of the defect is estimated by the conventional MFL method with the help of mathematical relation based on the references (Suresh et al., 2019). The RE is calculated to be approximately 5.55% for the conventional MFL method. From the results, it is evident that the sensitivity of the proposed optical sensor method is higher than the bimorph sensor method and approximately equal to MFL method. On the other hand, the sensitivity of the bimorph sensor method is lower

than that of the MFL method. To improve the sensitivity of the bimorph sensor method, the bimorph sensor must be optimally positioned on the cantilever beam. An accurate mathematical model to describe the optimum location of the bimorph sensor along with dynamic strain analysis is under development.

The presented results are obtained under laboratory-based conditions. The output responses are evaluated independently by operating one sensor at a time for each method. To overcome the limitations of a single sensor, multiple sensors are used in an array configuration. A crucial step in validating the effectiveness of the new integrated ILI is to
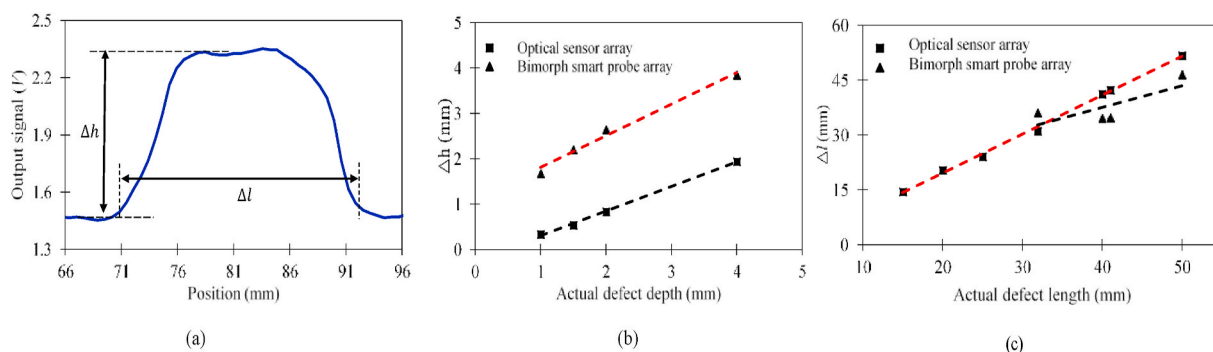
**Fig. 12.** The relationship between the output response and the defect size (a) definition of $\Delta h$ and $\Delta l$ when the defect is scanned with the proposed ILI method (b) $\Delta h$ with different depth defects and (c) $\Delta l$ with different length defects.
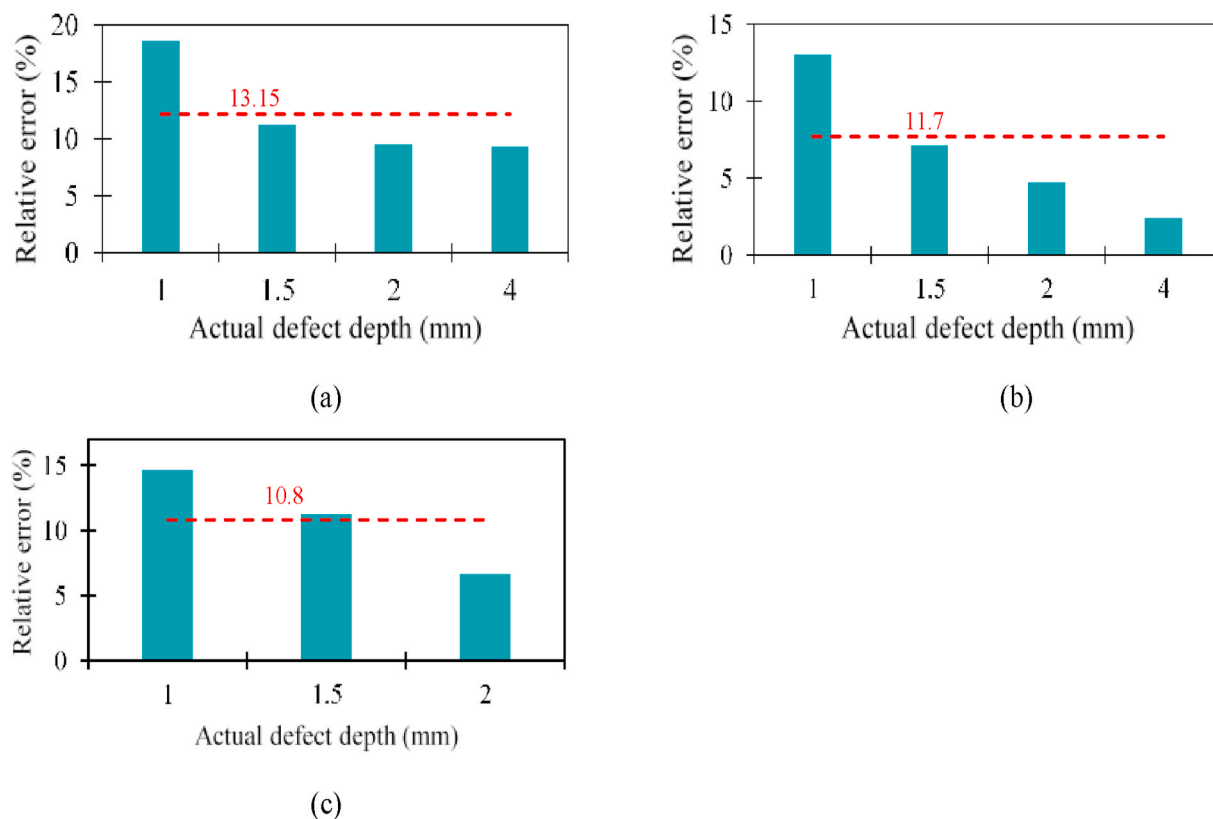


**Fig. 13.** Relative errors of the defect depth estimations (a) optical sensor method, (b) bimorph sensor method and (c) MFL sensor method.

**Table 5**
Performance of the different methods in estimation of the different depths of the defects.

| Method | Defects | Convex_1 | | | Metal loss_1 | | | Metal loss_2 | | | | Convex_2 | | |
|---|---|---|---|---|---|---|---|---|---|---|---|---|---|---|
| | | a1 | a2 | a3 | c1 | c2 | c3 | d1 | d2 | d3 | d4 | b1 | b2 | b3 |
| Optical sensor | Actual | 1 | 2 | 4 | 2 | 1.5 | 1 | 2 | 2 | 2 | 2 | 1.5 | 1 | 1.5 |
| | Estimated | 1.23 | 2.4 | 4.41 | 1.8 | 1.6 | 1.31 | 2.21 | 2.29 | 2.37 | 2.33 | 1.69 | 1.2 | 1.45 |
| | RE (%) | 18.6 | 16.6 | 9.29 | 11.1 | 6.2 | 23.66 | 9.5 | 12.6 | 15.6 | 14.1 | 11.24 | 16.6 | 3.4 |
| Bimorph sensor | Estimated | 1.15 | 2.1 | 4.1 | – | | | | | | | 1.4 | 1.2 | 1.54 |
| | RE (%) | 13 | 4.7 | 2.4 | | | | | | | | 7.1 | 16.6 | 2.6 |
| MFL | Estimated | – | | | 2.1 | 1.7 | 1.2 | 2.15 | 2.21 | 2.19 | 2.15 | – | | |
| | RE (%) | | | | 4.7 | 11.2 | 14.6 | 6.9 | 9.5 | 8.6 | 6.9 | | | |

obtain real-time field data. After successfully identifying and detecting the defects in segmented pipelines in laboratory conditions, the result of the integrated ILI method should be evaluated in real field application.

## 5. Field tests

A novel and low-cost smart PIG is designed and developed for the inspection of gas pipelines with the developed speed control system. The
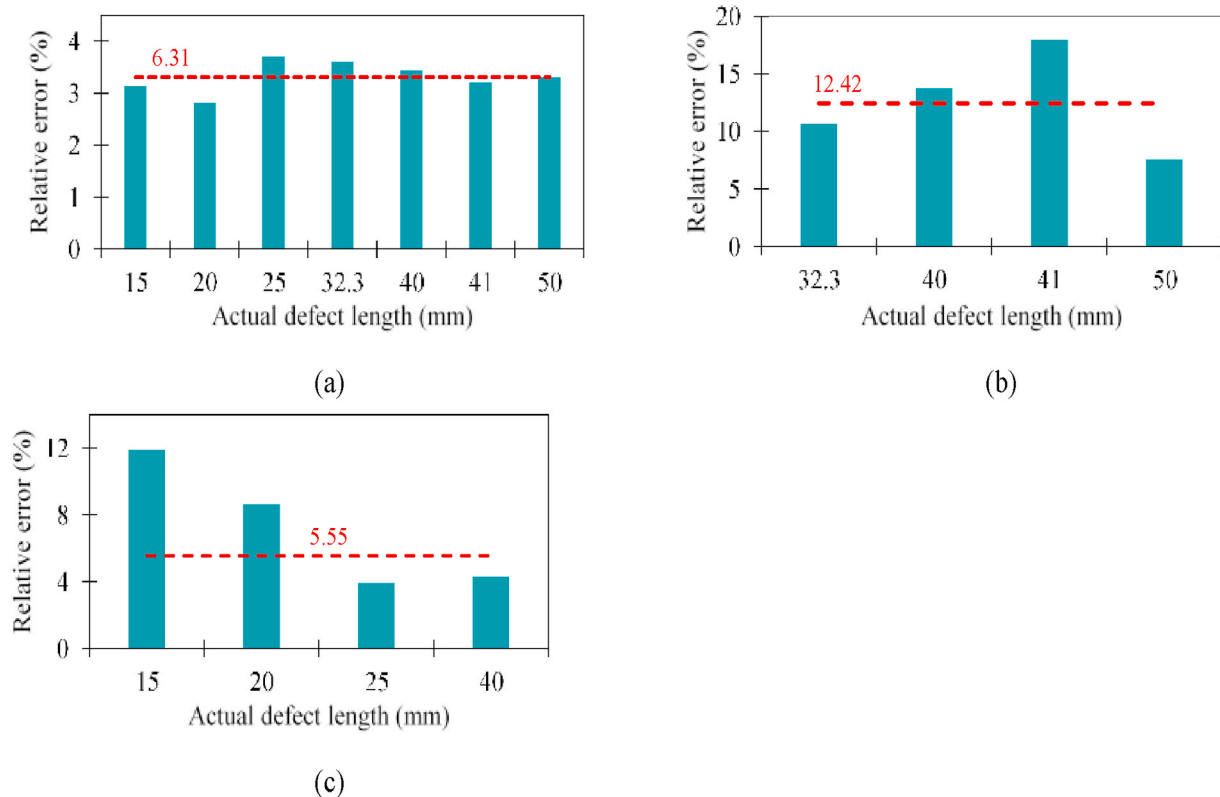
**Fig. 14.** Relative errors of the defect length estimations (a) optical sensor method, (b) bimorph sensor method and (c) MFL sensor method.

**Table 6**
Performance of the different methods in estimation of the different lenghts of the defects.

| Method | Defects | Convex defect_1 | | | Metal loss_1 | | | Metal loss_2 | | | | Convex defect_2 | | |
|---|---|---|---|---|---|---|---|---|---|---|---|---|---|---|
| | | a1 | a2 | a3 | c1 | c2 | c3 | d1 | d2 | d3 | d4 | b1 | b2 | b3 |
| Optical sensor | Actual | 32.3 | 41 | 50 | 40 | 40 | 40 | 20 | 20 | 25 | 15 | 40 | 40 | 40 |
| | Estimated | 31.15 | 42.35 | 51.71 | 41.24 | 40.43 | 41.10 | 20.41 | 20.75 | 24.1 | 14.54 | 41.87 | 41.38 | 41.95 |
| | RE (%) | 3.6 | 3.2 | 3.3 | 3.0 | 1.1 | 2.67 | 2.0 | 3.6 | 3.7 | 3.13 | 3.9 | 3.3 | 4.6 |
| Bimorph sensor | Estimated | 36.12 | 34.75 | 46.52 | – | | | | | | | 34.53 | 34.58 | 36.45 |
| | RE (%) | 10.6 | 17.9 | 7.5 | | | | | | | | 15.8 | 15.6 | 9.73 |
| MFL | Estimated | – | | | 40.9 | 41.05 | 41.8 | 21.5 | 21.9 | 26.03 | 17.04 | – | | |
| | RE (%) | | | | 2.2 | 1.05 | 4.3 | 6.9 | 8.6 | 3.9 | 11.9 | | | |

real field test results are presented and discussed.

## 5.1. Development of smart PIG and gas pipeline network

The field tests are conducted for an in-house pipeline network originally developed at the institute. The smart PIG designed by Smart Materials, Structures & Systems (SMSS) research group in the Department of Mechanical Engineering of Indian Institute of Technology Kanpur is shown in Fig. 15. The developed smart PIG consists of two parts: 1) an inspection system for pipelines and 2) a speed control system to maintain a uniform speed of the smart PIG. The smart PIG system comprises of four main modules: the integrated ILI modules (the optical, bimorph and MFL module), position tracer (odometer), power supply, and a DAQ unit. The role of the odometer is to measure the distance traveled by the smart PIG for the transverse interval considered. The speed of the smart PIG can be calculated based on the incremental distance between two such intervals. The odometer could also be used to trace the defect location. The power (direct current) is supplied to sensors through a 12 V battery made of lithium polymer battery cells. The power supply had a capacity of providing up to 70 Ah of continuous power to the sensors for a meaningful 10-h mission. Each module is

designed considering maneuverability and well connected to other modules through an articulated joint. A single data hub module is used for collecting data from 40 sensors, i.e., optical sensors-32, bimorph sensors-4 and Hall sensors-4. The smart PIG is equipped with a wireless robot tracking system with 5.1 GHz bandwidth through which records the current position of the PIG, and the defect position data. The smart PIG with the individually designed modules mounted along the axis-core weighed around 16 kg and the overall measured length of the integrated ILI method is about 110 cm.

The pipeline, which is used in the field test, is reported to have no defects. However, the presence of the bolted joint that is artificially installed on the test pipeline (with a 0.5 m distance) is considered as an abnormality for the test. Pipeline characteristics and operating conditions that are used for the field-test are as follows: inner diameter is 200 mm and thickness is 7 mm, pipeline length is 100 m, thrust: compressed air, working pressure inside the pipeline is 0.2 MPa, inspection speed of the smart PIG is set to 10 mm/s and inspection duration is about 2.77 h. The robot is designed to harvest the kinetic energy of the gas to propel itself inside the pipeline. Since the smart PIG flowed along with the fluid, there is no hindrance to fluid flow.

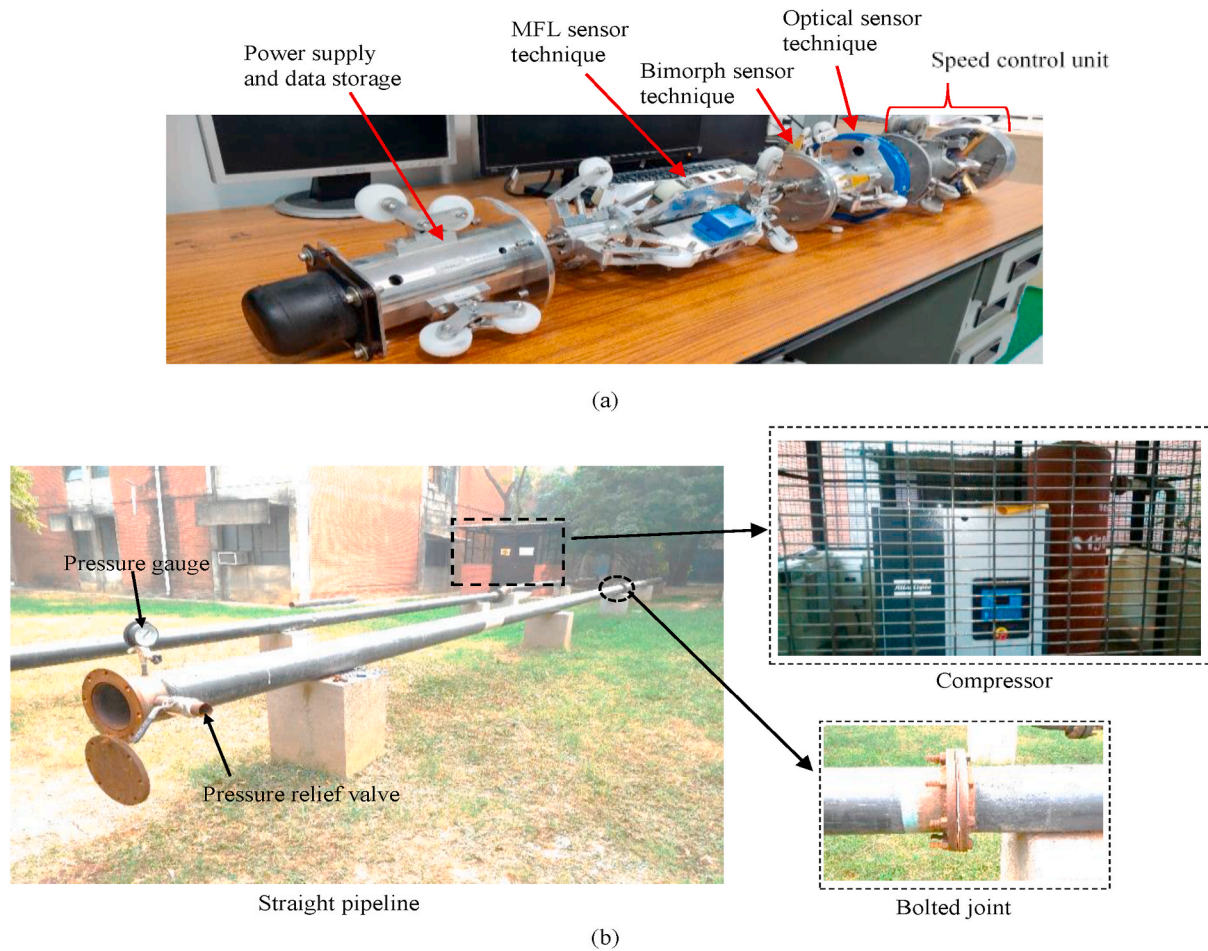For real-time, ILI applications and in terms of DAQ rate, storage, and

(a)



(b)

**Fig. 15.** The real filed test setup. (a) Image of the designed smart PIG for in-line application and (b) gas pipeline network.

advanced efficient wireless data transfer without time delay are used. The smart PIG is capable of being equipped with a wireless robot tracking systems such as X-bee (pro-S1 PCB antenna model), by which the position of the robot and locations of the probable defects can be obtained in real-time. Two X-bee modules can be installed to communicate with each other, where one can be used for the transmission and the other functions as a receiver. The transmitter X-bee should be mounted on the microcontroller board, and the receiver X-bee via RF (radio frequency) waves receives data using the ZigBee protocol. The receiver X-bee is possible to connect to another microcontroller, to transfer data to a PC using a LabVIEW interface. After preliminary verification of pipeline conditions by launching the testing robot, the smart PIG unit is launched at one end of the pipeline. The smart PIG is used to inspect the bolted joint using the proposed method. At the end of the inspection process, the smart PIG unit is recovered from another end of the pipeline. The raw data acquired during the inspection process was stored in a solid-state memory on board. The data were post-processed. The obtained results using the optical sensor array are presented in Fig. 16(a). In Fig. 16(a), there is also a line scan similar to the optical sensors plot. The output signals from 32 optical sensors of array signals are shown as a two-dimensional (2D) image. In the 2D image, the abscissa-axis represents the axial distance, and the ordinate-axis represents the number of optical sensor arrays (across the circumferential distance). The 2D image could be used for quick visual display of the inner surface of the pipeline. The image from the array sensor showed drastic changes at the location of the bolted joint. Fig. 16(b) shows the output response obtained from the bimorph sensor array. In Fig. 16, the location and size of the bolted joint is obvious. The estimated size of the bolted joint by the optical sensor array is calculated to be 48.7 mm using

optical method and 52.4 mm (4% error) by bimorph method. Results show that the proposed integrated ILI method can effectively detect bolted joint dimensions. However, the output sensor signals from both methods showed high voltage fluctuations as well as jumps in various locations, which may be due to the significant vibration or uneven speed of the smart PIG.

*5.2. Speed control system of the smart PIG*

The smart PIG works under highly pressurized gas pipelines, and thus the inspection tool can attain undesirably high travel speeds. The high travel speed leads to inconsistency in inspection due to mismatch with the sampling frequency of the sensors mounted on the inspection tool (see Fig. 15(a)). Reliable, complete, and high-quality data are directly dependent on the smart PIG speed. Oil pipelines with the incompressibility and lubricating features of liquid can prevent the sudden increase in the magnitude of velocity, unlike gas lines, that are highly prone to velocity surges due to the compressibility of gases. Therefore, it is prudent to place a speed control system attached to PIG to establish speed control primarily in natural gas pipelines as shown in Fig. 17.

The performance of several inspection systems directly depends upon the travel speed of the PIG, as it is strongly correlated with the scanning rate of the sensors. To get accurate inspection data, the velocity of the PIG should generally be in the range of 2–6 m/s in gas pipelines (Nguyen et al., 2001). Accordingly, an active control system is currently being used to control the cross-sectional area of the bypass depending upon the pressure differential between upstream and downstream and the flow rate in the pipeline (Zhu et al., 2014; Zhang et al., 2015). The
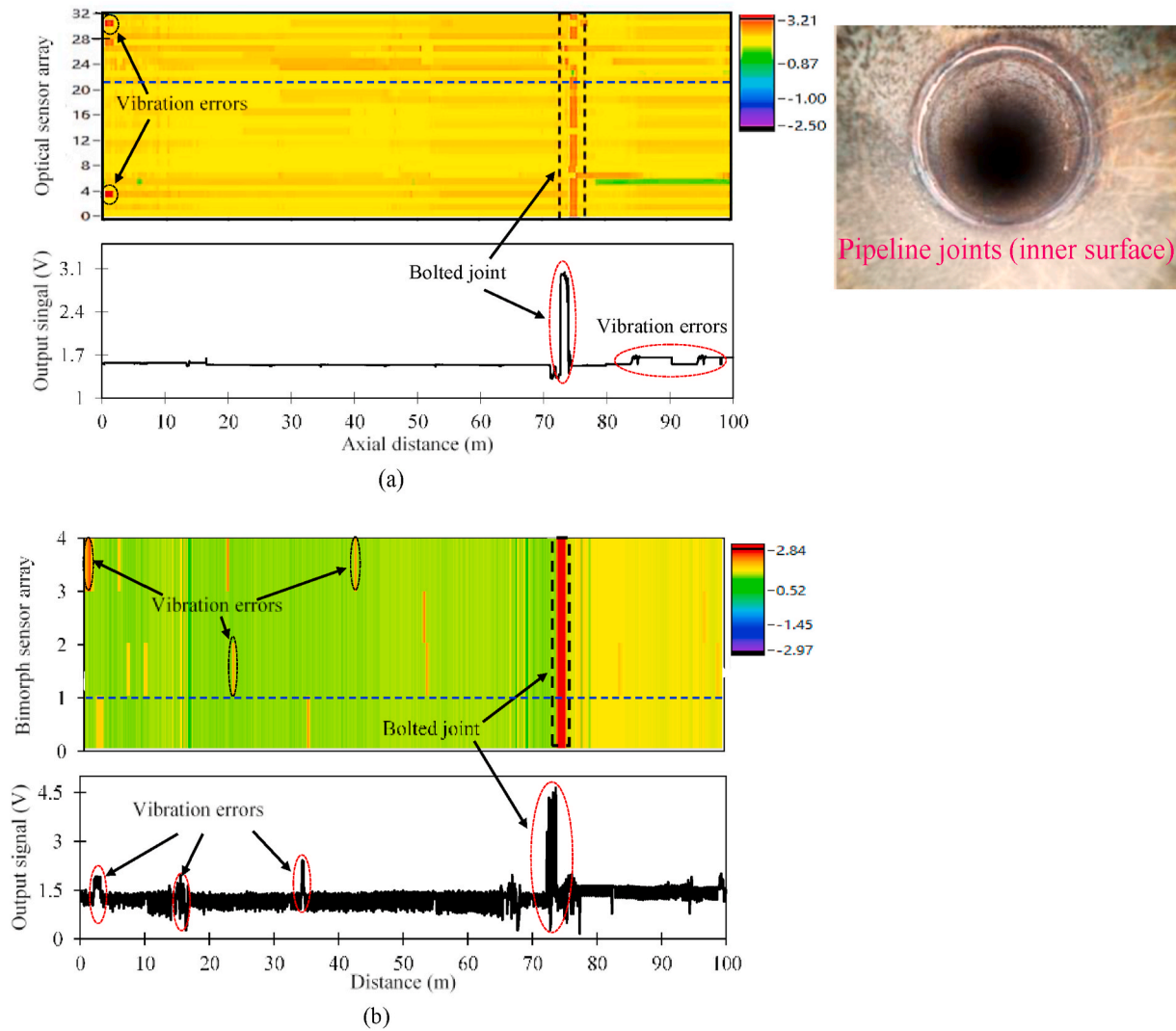
Pipeline joints (inner surface)

**Fig. 16.** Measured results of bolted joint signals detected by (a) optical sensor method and (b) bimorph sensor method.
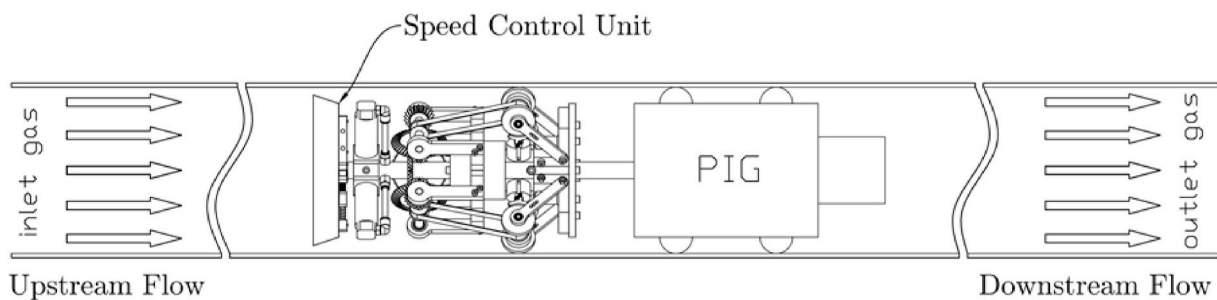


**Fig. 17.** Schematic view of the PIG with speed control unit inside a gas pipeline.

active speed control system involves complex electronic control of the bypass valve and suffers from a demerit of reaction time. Therefore, the sudden changes in the travel speed of the PIG cannot always be handled in an optimum response time.

The present system envisages a speed control mechanism for PIG using a hydro-mechanical brake system. A brake unit is attached to the PIG and moved in the pipeline to control the travel speed of the whole system. More specifically, the wheel on the brake unit is pressed against the pipeline wall using the suspension so as enable the roll of the wheel on the wall. The rotational kinetic energy of the wheel is harnessed to

pressurize the brake fluid in the system. The brake fluid pressure is transferred to act as a normal force on the brake wheel and, in turn, increases the frictional force and decreases the overall velocity of the PIG. The frictional force so generated will also reduce the angular speed of the brake wheel. This, in turn, will have an immediate effect on the hydraulic pressure build-up in the piston-cylinder assembly. Thus, the normal force acting on the brake wheel also changes immediately. All the above sequential steps create the closed-loop control system.

The hydro-mechanical solution described above is cost-effective, reliable, and most responsive with respect to any change in travel

speed due to the incompressibility of the brake fluid, which enables the transmission of pressure changes instantaneously. The novel feature of the present invention is that it is a passive, robust and light-weight hydro-mechanical system which can be customized in-line with the desired magnitude of travel velocity. The system design offers reliability and stability of all the sub-components up to a high-pressure magnitude (~2 MPa). The system design has a provision of bypass flow thus it does not create hindrance in the normal delivery or halt the transportation operation of natural gas through the pipelines.

Advancements in smart PIG technologies coupled with a growing research and development activities are expected to improve natural gas pipeline maintenance services. One such instance of the advanced technology is the development of a speed control system for smart PIG, to accurately identify and classify defects and leakage and metal loss/corrosion detection thereby enhancing the effectiveness of the inspection tool. When a robot moves in a highly pressurized gas pipeline, its velocity can be as high as 12–15 m/s. Such a high velocity is not beneficial for high-resolution scanning of the pipeline, which requires maximum speed up to 2–6 m/s. Also, due to slopes and curved trajectories, the motion of the robot varies non-uniformly inside the pipe. To circumvent both the problems, a new speed control system is developed, which exploits centrifugal rotation of an array of a spring-mass system to control hydraulic brakes and the area of the back plate to control bypass flow. As a result, the robot is able to move at a designed speed of about 3 m/s, along with a speed variation of about 0.5 m/s. The entire system does not require any electrical power and hence completely safe and robust for driving pipe inspection robots at a uniform slow speed in an inflammable environment.

As per report from the professional gas transportation in India, the inspection service (pigging) offered by the health monitoring companies cost approximately at the rate of $100 per km of pipe length. For 100 km of pipeline pigging, the service costs close to $10,000. The ILI prototype developed by us at the SMSS Laboratory, IIT Kanpur, costs $2054. For a full-fledged model, the total cost of production for 1 unit is approximately $6845. Thus, the proposed model serves as a better cost-effective solution than the existing health monitoring system.

*5.3. Study of chatter vibration response during pigging in the pipeline*

Several studies (Zhang et al., 2015, 2017; Qin and Cheng, 2020) have reported the phenomenon of chatter vibrations in the ILI tool moving in the natural gas pipelines. The basic design of conventional PIG comprises the body, sealing cups or discs, and sensing components. The sealing cups maintain complete contact with the inner surface of the pipeline to achieve desired differential pressure condition. However, the frictional force between the sealing cup and the inner surface of the pipe leads to self-excited vibration into the system (Zhang et al., 2020) which manifests as chatter vibration. An experiment has been carried on our in-house pipeline network to study the transmission and impact of chatter vibration on the pipeline when the smart PIG moves through the pipe. To measure the natural frequencies, close to the fundamental mode of the pipeline, an impact hammer test has been performed in which the power spectral density and spectrogram analysis give the natural frequency of the fundamental mode at 10.9 Hz, followed by the subsequent modes at 14.8 Hz and 17.6 Hz, respectively.

The schematic and the field test setup of the experiment have been shown in Fig. 18. The chatter vibration response originating due to smart PIG movement in the pipe has been captured and shown in Fig. 19. Using a power spectral density estimate, it has been observed that the vibration transmitted to the pipeline has dominating frequencies of 304 Hz and 848 Hz, respectively. Further analysis using spectrogram reveals that, though there is a presence of white noise in the signal, the frequency of 304 Hz is most prominent when the smart PIG passes through the sensor location, indicating that moving PIG induces and transmits a chatter vibration which is far above the fundamental frequency of the pipeline.

An important difference between the smart PIG and conventional PIG is the design of support system. In the case of conventional PIG, there is a sliding contact with the internal surface of the pipeline. On the other hand, the smart PIG comprises wheel suspension assembly to maintain rolling contact with the inner surface of the pipeline reducing the possibility of stick-slip condition.

## 6. Conclusions

This paper presented an innovative defect detection and localization method in gas pipelines using integrated in-line inspection (ILI) method. The design principles of the development of the smart PIG with integrated ILI methods such as optical sensor and bimorph sensor arrays are described in detail. The sensors are developed to identify the positions and sizes of defects in the pipeline. Laboratory-based tests are first conducted on the segmented pipeline specimen. The results confirmed that the proposed method can accurately detect deliberately introduced convexities and metal loss defects. Laboratory tests are followed by real-time field tests that involved the passage of the integrated ILI method based smart PIG for a total distance of 100 m through a 200 mm inner diameter pipe. A speed control module is also incorporated to maintain a constant speed of the unit with reference to the fluid stream velocity. The observations from the field tests are consistent with the lab-scale results and validate the effectiveness of the smart PIG in detecting defects in a single run. The primary outcomes of the current research, which highlight the significance and recommendations can be listed as:

- Integrated in-line inspection method are proposed to detect and localize defects in gas pipelines,
- A low-cost smart PIG is developed and applied to inspect bolted joint in the real field test,
- The speed control system is designed to maintain the speed of the smart PIG and eliminate errors caused by speed spikes,
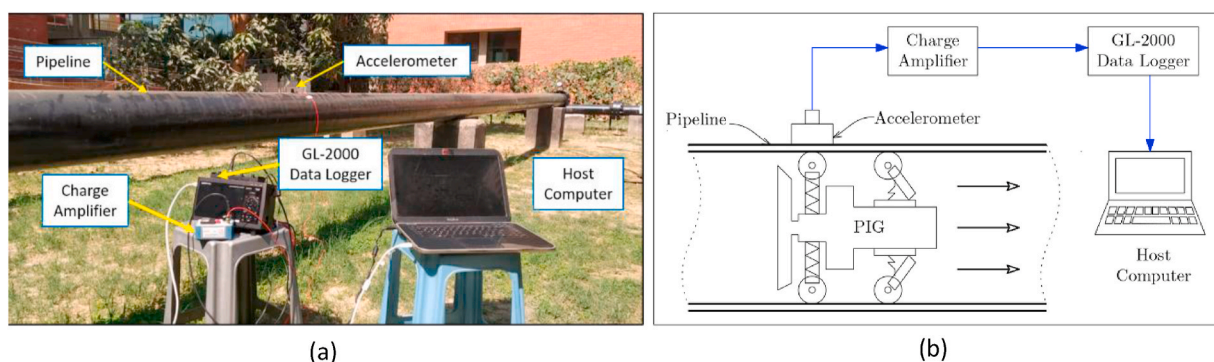


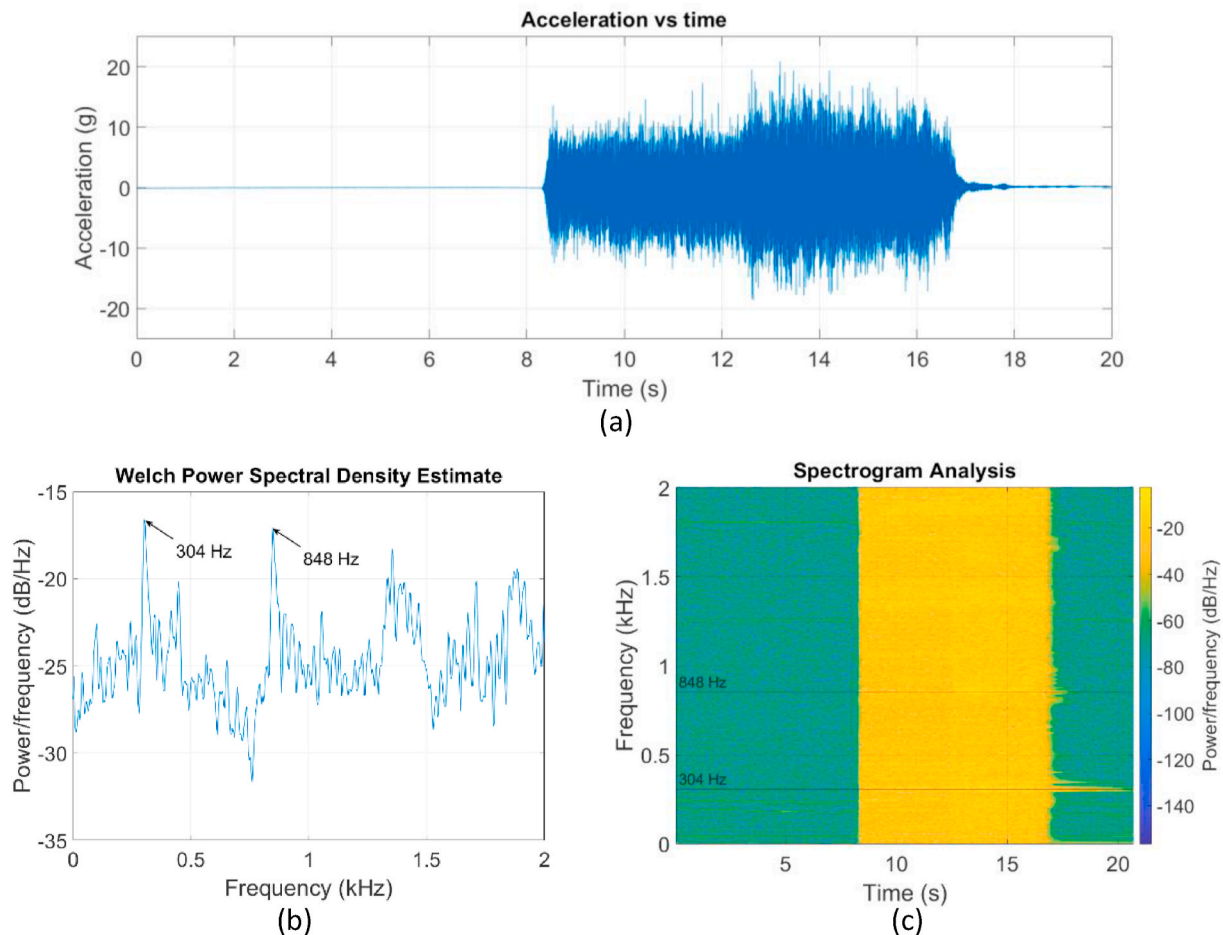**Fig. 18.** (a) Field test setup of the experiment and (b) schematic in the form of a system block diagram.

**Fig. 19.** The chatter vibration signal originating due to smart PIG movement in the pipeline: (a) Acceleration, (b) power spectral density and (c) spectrogram.

- The dominating frequency of chatter vibration of smart PIG in experiment is estimated to be 304 Hz, which is far above from the fundamental frequency mode of the pipeline,
- The outcomes indicate the proposed ILI method such as optical and bimorph sensors can effectively estimate the defect size and accurately identify the defect position.

The current research work is partially motivated by the increasing demand from gas industry and presented a candidate method for the in-line and real-time pipeline inspection. As a part of future development, the performance of the proposed method requires to be evaluated for real-world pipeline networks with multiple confirmed defects in operational conditions. Also, the hydro-mechanical based speed control system can be modified to have better control of leakage, and thus the hydraulic system can be utilized in a more effective manner. This will not only improve the responsiveness of the system but also enhance the life of the overall brake unit as well. Further development can be obtained by a suitable choice of material to be used for manufacturing to get further weight reduction of the complete system.

**Credit roles**

Santhakumar Sampath: Investigation, Methodology, Sensor design, Experimental analysis, Writing – original draft. Kanhaiya Lal Chaurasiya: Methodology, Experimental analysis, Writing – review & editing. Pouria Aryan: Writing – review & editing. Bishakh Bhattacharya: Supervision, Conceptualization, Writing – review & editing.

**Declaration of competing interest**

The authors declare that they have no known competing financial interests or personal relationships that could have appeared to influence the work reported in this paper.

**References**

Agarwal, V., Harutoshi, O., Kentarou, N., Bhattacharya, B., 2011. Inspection of pipe inner surface using advanced pipe crawler robot with PVDF sensor based rotating probe. Sensors & Transducers 127, 45.

Amaya-Gómez, R., Sánchez-Silva, M., Bastidas-Arteaga, E., Schoefs, F., Munoz, F., 2019. Reliability assessments of corroded pipelines based on internal pressure–A review. Eng. Fail. Anal. 98, 190–214.

Askari, M., Aliofkhazraei, M., Afroukhteh, S., 2019. A comprehensive review on internal corrosion and cracking of oil and gas pipelines. J. Nat. Gas Sci. Eng. 102971.

Beckmann, P., Spizzichino, A., 1987. The Scattering of Electromagnetic Waves from Rough Surfaces. Artech House, Inc., Norwood, MA, p. 511, 1987.

Bickerstaff, R., Vaughn, M., Stoker, G., Hassard, M., Garrett, M., 2002. Review of Sensor Technologies for In-Line Inspection of Natural Gas Pipelines. Sandia National Laboratories, Albuquerque, NM.

Biswal, A.R., Roy, T., Behera, R.K., 2017. Optimal vibration energy harvesting from non-prismatic axially functionally graded piezolaminated cantilever beam using genetic algorithm. J. Intell. Mater. Syst. Struct. 28, 1957–1976.

Bubenik, T., Nestlroth, J., Eiber, R., Saffell, B., 1997. Magnetic Flux Leakage (MFL) Technology for Natural Gas Pipeline inspection. NDT E Int. 1, 36.

Caleyo, F., Alfonso, L., Espina-Hernandez, J.H., Hallen, J., 2007. Criteria for performance assessment and calibration of in-line inspections of oil and gas pipelines. Meas. Sci. Technol. 18, 1787.

Canavese, G., Scaltrito, L., Ferrero, S., Pirri, C., Cocuzza, M., Pirola, M., Corbellini, S., Ghione, G., Ramella, C., Verga, F., 2015. A novel smart caliper foam pig for low-cost pipeline inspection—Part A: design and laboratory characterization. J. Petrol. Sci. Eng. 127, 311–317.

Dhar, S., Shukla, P.R., 2015. Low carbon scenarios for transport in India: Co-benefits analysis. Energy Pol. 81, 186–198.

Dong, J., Zhang, H., Liu, S., 2019. 3D printed bio-inspired sealing disc of pipeline inspection gauges (PIGs) in small diameter pipeline. J. Nat. Gas Sci. Eng. 61, 344–356.

Duran, O., Althoefer, K., Seneviratne, L.D., 2002. State of the art in sensor technologies for sewer inspection. IEEE Sensor. J. 2, 73–81.

O. Duran, K. Althoefer, L.D. Seneviratne, A sensor for pipe inspection: model, analysis and image extraction, in, IEEE, pp. III-597.

Ege, Y., Coramik, M., 2018. A new measurement system using magnetic flux leakage method in pipeline inspection. Measurement 123, 163–174.

Eybpoosh, M., Berges, M., Noh, H.Y., 2017. An energy-based sparse representation of ultrasonic guided-waves for online damage detection of pipelines under varying environmental and operational conditions. Mech. Syst. Signal Process. 82, 260–278.

Ginzel, R., Kanters, W., 2002. Pipeline corrosion and cracking and the associated calibration considerations for same side sizing applications. NDT. net 7, 1435–4934.

Gloria, N., Areiza, M., Miranda, I., Rebello, J., 2009. Development of a magnetic sensor for detection and sizing of internal pipeline corrosion defects. NDT E Int. 42, 669–677.

Hawari, A., Alamin, M., Alkadour, F., Elmasry, M., Zayed, T., 2018. Automated defect detection tool for closed circuit television (cctv) inspected sewer pipelines. Autom. ConStruct. 89, 99–109.

Ho, M., El-Borgi, S., Patil, D., Song, G., 2020. Inspection and monitoring systems subsea pipelines: a review paper. Struct. Health Monit. 19, 606–645.

Iqbal, H., Tesfamariam, S., Haider, H., Sadiq, R., 2017. Inspection and maintenance of oil & gas pipelines: a review of policies. Structure and Infrastructure Engineering 13, 794–815.

Kim, H.M., Heo, C.G., Cho, S.H., Park, G.S., 2018. Determination scheme for accurate defect depth in underground pipeline inspection by using magnetic flux leakage sensors. IEEE Trans. Magn. 54, 1–5.

Kursu, O., Kruusing, A., Pudas, M., Rahkonen, T., 2009. Piezoelectric bimorph charge mode force sensor. Sensor Actuator Phys. 153, 42–49.

Li, Y., Tian, G.Y., Ward, S., 2006. Numerical simulation on magnetic flux leakage evaluation at high speed. NDT E Int. 39, 367–373.

Li, X., Zhang, S., Liu, S., Jiao, Q., Dai, L., 2015a. An experimental evaluation of the probe dynamics as a probe pig inspects internal convex defects in oil and gas pipelines. Measurement 63, 49–60.

Li, X., Zhang, S., Liu, S., Zhu, X., Zhang, K., 2015b. Experimental study on the probe dynamic behaviour of feeler pigs in detecting internal corrosion in oil and gas pipelines. J. Nat. Gas Sci. Eng. 26, 229–239.

Li, Y., Cai, R., Yan, B., Zainal Abidin, I.M., Jing, H., Wang, Y., 2018. A capsule-type electromagnetic acoustic transducer for fast screening of external corrosion in nonmagnetic pipes. Sensors 18, 1733.

Lim, S.-H., Choi, J., Horowitz, R., Majumdar, A., 2005. Design and fabrication of a novel bimorph microoptomechanical sensor. Journal of Microelectromechanical Systems 14, 683–690.

Mikhaylov, A., Gobov, Y.L., Smorodinskii, Y.G., Korzunin, G., 2020. Electromagnetic acoustic transducers for non-destructive testing of main pipelines. In: Journal of Physics: Conference Series. IOP Publishing, 012012.

Nakhli Mahal, H., 2020. Signal Processing Techniques for Enhancement of Defect Detection in Ultrasonic Guided Waves Inspection of Pipelines. Brunel University London.

Nguyen, T.T., Kim, S.B., Yoo, H.R., Rho, Y.W., 2001. Modeling and simulation for pig flow control in natural gas pipeline. KSME Int. J. 15, 1165–1173.

Ogai, H., Bhattacharya, B., 2018. Pipe Inspection Robots for Structural Health and Condition Monitoring. Springer.

Okamoto Jr., J., Adamowski, J.C., Tsuzuki, M.S., Buiochi, F., Camerini, C.S., 1999. Autonomous system for oil pipelines inspection. Mechatronics 9, 731–743.

Peng, X., Anyaoha, U., Liu, Z., Tsukada, K., 2020. Analysis of magnetic-flux leakage (MFL) data for pipeline corrosion assessment. IEEE Trans. Magn. 56, 1–15.

Qin, G., Cheng, Y.F., 2020. Failure pressure prediction by defect assessment and finite element modelling on natural gas pipelines under cyclic loading. J. Nat. Gas Sci. Eng. 81, 103445.

K. Reber, M. Beller, H. Willems, O.A. Barbian, A new generation of ultrasonic in-line inspection tools for detecting, sizing and locating metal loss and cracks in transmission pipelines, in, IEEE, pp. 665-671.

Saeidbakhsh, M., Rafeeyan, M., Ziaei-Rad, S., 2009. Dynamic analysis of small pigs in space pipelines. Oil & Gas Science and Technology-Revue de l'IFP 64, 155–164.

Salama, M.M., Nestleroth, B.J., Maes, M.A., Dash, C., 2013. Characterization of the uncertainties in the inspection results of ultrasonic intelligent pigs. In: International Conference on Offshore Mechanics and Arctic Engineering. American Society of Mechanical Engineers. V003T003A044.

S. Sampath, R. Dhayalan, A. Kumar, N. Kishore, H. Sohn, Evaluation of Material Degradation Using Phased Array Ultrasonic Technique with Full Matrix Capture, Engineering Failure Analysis, 120 105118.

Sampath, S., Bhattacharya, B., Aryan, P., Sohn, H., 2019. A real-time, non-contact method for in-line inspection of oil and gas pipelines using optical sensor array. Sensors 19, 3615.

Sampath, S., Sohn, H., Bhattacharya, B., 2020. Development of Novel Integrated In-Line Inspection Techniques for Pipeline Inspection. SPIE.

Smith, J.W., Hay, B.R., 2000. Magnetic Flux Leakage Inspection Tool for Pipelines. Google Patents.

Sophian, A., Tian, G.Y., Taylor, D., Rudlin, J., 2002. Design of a pulsed eddy current sensor for detection of defects in aircraft lap-joints. Sensor Actuator Phys. 101, 92–98.

Suresh, V., Abudhahir, A., Daniel, J., 2019. Characterization of defects on ferromagnetic tubes using magnetic flux leakage. IEEE Trans. Magn. 55, 1–10.

Ulapane, N., Alempijevic, A., Vidal Calleja, T., Valls Miro, J., 2017. Pulsed eddy current sensing for critical pipe condition assessment. Sensors 17, 2208.

Vanaei, H., Eslami, A., Egbewande, A., 2017. A review on pipeline corrosion, in-line inspection (ILI), and corrosion growth rate models. Int. J. Pres. Ves. Pip. 149, 43–54.

Varela, F., Yongjun Tan, M., Forsyth, M., 2015. An overview of major methods for inspecting and monitoring external corrosion of on-shore transportation pipelines, Corrosion Engineering. Sci. Technol. 50, 226–235.

Wang, Z., Wang, S., Wang, Q., Zhao, W., Huang, S., 2020. Development of a helical Lamb wave electromagnetic acoustic transducer for pipeline inspection. IEEE Sensor. J. 20 (17), 9715–9723.

Wu, L., Yao, K., Shi, P., Zhao, B., Wang, Y.-S., 2020. Influence of inhomogeneous stress on biaxial 3D magnetic flux leakage signals. NDT E Int. 109, 102178.

Xie, M., Tian, Z., 2018. A review on pipeline integrity management utilizing in-line inspection data. Eng. Fail. Anal. 92, 222–239.

Xie, L., Gao, B., Tian, G., Tan, J., Feng, B., Yin, Y., 2019. Coupling pulse eddy current sensor for deeper defects NDT. Sensor Actuator Phys. 293, 189–199.

Xie, S., Duan, Z., Li, J., Tong, Z., Tian, M., Chen, Z., 2020. A novel magnetic force transmission eddy current array probe and its application for nondestructive testing of defects in pipeline structures. Sensor Actuator Phys. 112030.

Xue, Z., Fan, M., Cao, B., Wen, D., 2020. A fast numerical method for the analytical model of pulsed eddy current for pipelines. Insight-Non-Destructive Testing and Condition Monitoring 62, 27–33.

Yu, J., Lee, J.G., Park, C.G., Han, H.S., 2005. An off-line navigation of a geometry PIG using a modified nonlinear fixed-interval smoothing filter. Contr. Eng. Pract. 13, 1403–1411.

Zhang, H., Zhang, S., Liu, S., Zhu, X., Tang, B., 2015. Chatter vibration phenomenon of pipeline inspection gauges (PIGs) in natural gas pipeline. J. Nat. Gas Sci. Eng. 27, 1129–1140.

Zhang, H., Zhang, S., Liu, S., Wang, Y., 2017. Collisional vibration of PIGs (pipeline inspection gauges) passing through girth welds in pipelines. J. Nat. Gas Sci. Eng. 37, 15–28.

Zhang, H., Dong, J., Cui, C., Liu, S., 2020. Stress and strain analysis of spherical sealing cups of fluid-driven pipeline robot in dented oil and gas pipeline. Eng. Fail. Anal. 108, 104294.

Zhao, F., Chen, D., Pu, Z., Wang, J., 2020. A new research method for corrosion defect in metal pipeline by using pulsed eddy current. In: Pressure Vessels and Piping Conference. American Society of Mechanical Engineers. V007T007A012.

Zhu, X., Zhang, S., Tan, G., Wang, D., Wang, W., 2014. Experimental study on dynamics of rotatable bypass-valve in speed control pig in gas pipeline. Measurement 47, 686–692.

Zhu, X., Jiao, Q., Li, X., Zhang, S., Liu, S., 2018. Experimental research on the precision of wheeled caliper arm for measuring pipeline deformation. Measurement 127, 15–20.